

Incommensurate Spin Fluctuations in the Spin-Triplet Superconductor Candidate UTe_2 Chunruo Duan,¹ Kalyan Sasmal,² M. Brian Maple,² Andrey Podlesnyak³,Jian-Xin Zhu⁴, Qimiao Si,¹ and Pengcheng Dai^{1,*}¹*Department of Physics and Astronomy, Rice Center for Quantum Materials, Rice University, Houston, Texas 77005, USA*²*Department of Physics, University of California, San Diego, California 92093, USA*³*Neutron Scattering Division, Oak Ridge National Laboratory, Oak Ridge, Tennessee 37831, USA*⁴*Theoretical Division and Center for Integrated Nanotechnologies, Los Alamos National Laboratory, Los Alamos, New Mexico 87545, USA*

(Received 5 July 2020; revised 27 September 2020; accepted 2 November 2020; published 1 December 2020)

Spin-triplet superconductors are of extensive current interest because they can host topological state and Majorana fermions important for quantum computation. The uranium-based heavy-fermion superconductor UTe_2 has been argued as a spin-triplet superconductor similar to UGe_2 , $URhGe$, and $UCoGe$, where the superconducting phase is near (or coexists with) a ferromagnetic (FM) instability and spin-triplet electron pairing is driven by FM spin fluctuations. Here we use neutron scattering to show that, although UTe_2 exhibits no static magnetic order down to 0.3 K, its magnetism in the $[0, K, L]$ plane is dominated by incommensurate spin fluctuations near an antiferromagnetic ordering wave vector and extends to at least 2.6 meV. We are able to understand the dominant incommensurate spin fluctuations of UTe_2 in terms of its electronic structure calculated using a combined density-functional and dynamic mean-field theory.

DOI: [10.1103/PhysRevLett.125.237003](https://doi.org/10.1103/PhysRevLett.125.237003)

Superconductivity occurs in many metals when electrons form coherent Cooper pairs below the superconducting transition temperature T_c [1]. In conventional and most unconventional superconductors, electron Cooper pairs in the superconducting state form antiparallel spin singlets with the total spin $S = 0$ [2–6]. However, electrons in the superconducting state can also form parallel spin-triplet Cooper pairs [7–9], analogous to the equal spin pairing state in superfluid 3He [10]. Pauli's exclusion principle can be fulfilled for both singlet and triplet Cooper pairs by adjusting the symmetry of the orbital part of the wave function. For the spin-singlet pairing state, the orbital wave function has even parity (symmetric) with orbital angular momentum $L = 0$ (s wave), 2 (d wave), etc. For the spin-triplet state, the orbital wave function has odd parity (antisymmetric) with orbital angular momentum $L = 1$ (p wave), 3 (f wave), etc. [8,9]. While most unconventional superconductors have spin-singlet pairing associated with antiferromagnetic (AF) spin fluctuations [2–6], spin-triplet superconductors are rare, and the superconductivity is believed to be driven by longitudinal ferromagnetic (FM) spin fluctuations [7–9]. Since spin-triplet superconductors are intrinsically topological [11–14] and can host Majorana fermions important for quantum computation [15,16], it is important to understand a spin-triplet superconductor candidate by determining the associated spin fluctuations.

In spin-triplet superconductors such as UGe_2 [17], $URhGe$ [18], and $UCoGe$ [19], superconductivity arises through suppression of the static FM order [17] or coexists with static FM order [18,19]. Inelastic neutron scattering

(INS) experiments find clear evidence of FM spin fluctuations in $URhGe$ [20] and $UCoGe$ [21]. For the spin-triplet superconductor candidate Sr_2RuO_4 [8], where the material is paramagnetic at all temperatures and superconductivity does not coexist with static FM order, magnetism is dominated by incommensurate spin fluctuations arising from Fermi surface nesting of itinerant electrons [22–24], although weak FM spin fluctuations are also observed [25]. Similarly, although considerable evidence exists for spin-triplet superconductivity in UPt_3 [26–28], its superconductivity appears to be associated with AF order and spin fluctuations instead of FM spin fluctuations [29,30].

Recently, UTe_2 has been identified as a new spin-triplet superconductor with $T_c \approx 1.6$ K [31–34]. UTe_2 has an orthorhombic unit cell with space group $Immm$, where the U atoms form parallel ladders along the a axis inside trigonal prisms of Te atoms [Fig. 1(a)] [35]. The shortest U–U bond is along the rung of the ladder in the c -axis direction, while the easy axis of the U spins is along the a axis. The symmetry operation that connects one ladder to its nearest neighbor is the body-center $(\frac{1}{2}, \frac{1}{2}, \frac{1}{2})$ translation. A Curie-Weiss fit to the magnetic susceptibility data reveals an effective moment per U atom close to the $5f^2$ or $5f^3$ free ion value at high temperature [32]. No long-range magnetic order has been reported down to 0.25 K [31–36]. Instead, a sudden increase in the magnetic susceptibility below 10 K in response to a magnetic field applied parallel to the a axis resembles the quantum critical behavior of metallic ferromagnets, indicating strong FM spin fluctuations along the a axis [31]. This suggests that UTe_2 sits at the paramagnetic

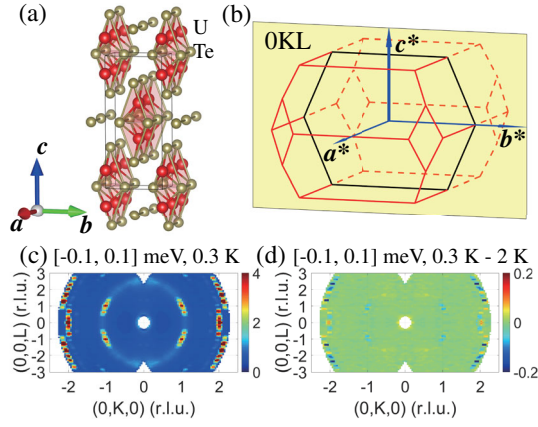


FIG. 1. (a) The crystal structure of UTe_2 . The first Brillouin zones (BZ) is sketched in (b), with the edges behind the $(0, K, L)$ plane plotted as dashed lines. The reciprocal space is labeled as \mathbf{a}^* , \mathbf{b}^* , \mathbf{c}^* . (c) The diffraction pattern of UTe_2 in the $(0, K, L)$ plane at $T = 0.3$ K. The integration range along the H direction is from -0.1 to 0.1 reciprocal lattice units (r.l.u.), and along energy is from -0.1 to 0.1 meV. (d) The temperature difference spectra between 0.3 and 2 K. The BZs are indicated by white solid lines in (c) and (d).

end of a series of FM heavy-fermion superconductors including UGe_2 [17], URhGe [18], and UCoGe [19]. At the FM end, the compound UGe_2 is a pressure-induced superconductor with optimal $T_c \approx 0.5$ K at 1.2 GPa [37,38]. Moving from UGe_2 to URhGe , superconductivity occurs at ambient pressure below $T_c \approx 0.25$ K and coexists with static FM order below a Curie temperature $T_C \approx 9.5$ K [18]. Finally, UCoGe has coexisting superconductivity and FM order with increased $T_c \approx 0.425$ K and decreased $T_C \approx 3$ K, respectively [19].

The scenario that UTe_2 is a candidate spin-triplet superconductor [31,32] is supported by a growing list of observations. These include the upper critical fields H_{C2} that exceed the Pauli limits along all crystallographic directions [33,34], temperature independent ^{125}Te Knight shift across T_c in nuclear magnetic resonance measurements [31], coexisting FM spin fluctuations and superconductivity [36,39], signatures of chiral superconductivity [40], and breaking of time reversal symmetry expected for a spin-triplet superconductor [41]. There are also theoretical [42] and experimental [43] efforts to understand the underlying electronic structure of UTe_2 .

In this Letter, we use INS to probe the wave vector and energy dependence of spin fluctuations of UTe_2 in the $[0, K, L]$ plane. In addition to confirming that UTe_2 exhibits no static magnetic order down to 0.3 K, we discovered that the dominant spin fluctuations in UTe_2 are three-dimensional (3D) in reciprocal space, centered at the incommensurate wave vector $\mathbf{Q} = (0, \pm(K + 0.57), 0)$ ($K=0, 1$) and extend to energies of at least $E=2.6$ meV. FM spin fluctuations, if present, are much weaker than the incommensurate spin fluctuations. Based on density-functional theory (DFT) in

the generalized gradient approximation [44], combined with dynamical mean-field theory (DMFT) calculations [45–48], we understand the dominant incommensurate spin fluctuations by showing that the associated wave vector is approximately consistent with the AF wave vector of the Ruderman-Kittel-Kasuya-Yosida (RKKY) interaction between the $5f$ moments. Therefore, in addition to a FM instability, incommensurate (close to AF) spin fluctuations must also be considered to unveil the magnetic and superconducting properties of UTe_2 .

Our INS experiments were carried out at the Cold Neutron Chopper Spectrometer (CNCS) at Oak Ridge National Laboratory. The momentum transfer \mathbf{Q} in 3D reciprocal space is defined as $\mathbf{Q} = H\mathbf{a}^* + K\mathbf{b}^* + L\mathbf{c}^*$, where H , K , and L are Miller indices and $\mathbf{a}^* = \hat{\mathbf{a}}2\pi/a$, $\mathbf{b}^* = \hat{\mathbf{b}}2\pi/b$, and $\mathbf{c}^* = \hat{\mathbf{c}}2\pi/c$ with $a = 4.16$, $b = 6.12$, and $c = 13.95$ Å of the orthorhombic lattice [35]. Single crystals of UTe_2 were prepared using the chemical vapor transport method with I_2 as the transport media (see Supplemental Material [49]). The crystals are naturally cleaved along the ab plane and form small flakes of about 0.5 – 1 mm thick. The typical dimension of the crystals in the ab plane is from 1 to 2 mm and the mass is in the range of 10 – 30 mg. We coaligned 61 pieces (total mass 0.7 g) of single crystals on oxygen-free Cu plates using a Laue x-ray machine to check the orientation of each single crystal. The sample assembly is aligned in the $[0, K, L]$ scattering plane as shown in the black frame of Fig. 1(b) and mounted inside a He^3 refrigerator. Most of our measurements were carried out with $E_i = 3.37$ meV on CNCS at different temperatures.

Figure 1(c) shows a map of reciprocal space in the $[0, K, L]$ scattering plane at 0.3 K and elastic position. We see nuclear Bragg peaks at the expected $(0, \pm 1, \pm 1)$, $(0, \pm 2, 0)$, and $(0, \pm 2, \pm 2)$ positions. The spread of the Bragg peaks along the powder ring direction indicates a broad sample mosaic of $\sim 15^\circ$. To search for possible static FM or AF magnetic order, we show in Fig. 1(d) the temperature difference plot between 0.3 and 2 K and find no evidence of intensity gain anywhere within the probed reciprocal space. We therefore conclude that UTe_2 does not exhibit static FM or AF order down to 0.3 K, consistent with earlier work [31–34,36].

Despite the absence of long-range magnetic order, INS experiments on UTe_2 reveal clear evidence for excitations at finite energy transfers. Figures 2(a)–2(d) show 2D images of constant-energy cuts in the $[0, K, L]$ plane at different energies below T_c ($T = 0.3$ K). At $E = 0.4 \pm 0.1$ meV, we see clear excitations at incommensurate wave vectors $\mathbf{Q}_{\text{IC}} = (0, \pm 0.57, 0)$ and a possible signal at FM wave vectors $\mathbf{Q}_{\text{FM}} = (0, \pm 1, \pm 1)$. On increasing energies to $E = 1 \pm 0.1$, 1.3 ± 0.1 , and 1.9 ± 0.1 meV, we see excitations at $\mathbf{Q}_{\text{IC}} = (0, \pm(K + 0.57), 0)$ with $K = 0, 1$ and no scattering at \mathbf{Q}_{FM} [Figs. 2(b)–2(d)]. FM spin waves from a single crystal assembly with $\sim 15^\circ$ mosaic cannot give rise to these excitations [49].

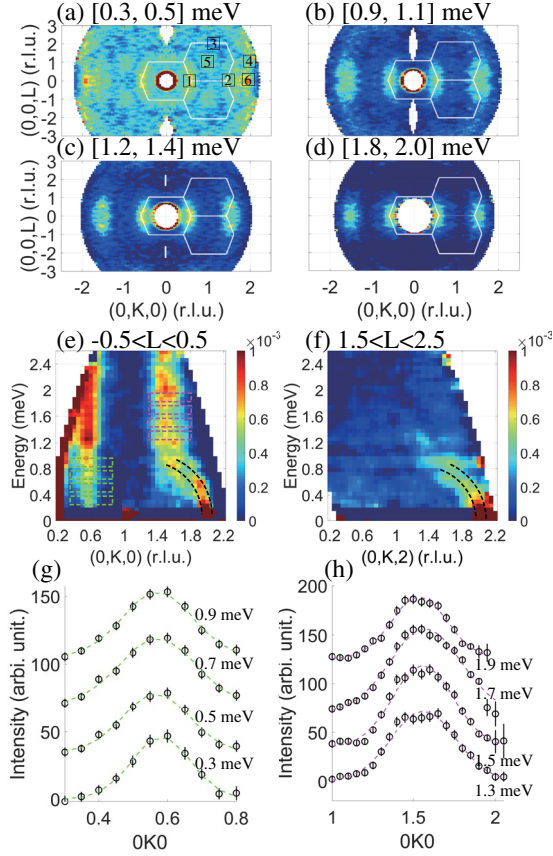


FIG. 2. Images of 2D constant-energy cuts in the $(0, K, L)$ scattering plane at $T = 0.3$ K. Along the H direction, the integration range is from -0.1 to 0.1 r.l.u., while the energy ranges are (a) 0.3 – 0.5 , (b) 0.9 – 1.1 , (c) 1.2 – 1.4 , and (d) 1.8 – 2.0 meV. The BZs are indicated by white solid lines. In subplot (a), black squares labeled from 1 to 6 indicate the \mathbf{Q} ranges of the 1D cuts along energy plotted in Figs. 3(a)–3(f), respectively. $\chi''(E, \mathbf{Q})$ integrated in (e) $-0.5 < L < 0.5$ and (f) $1.5 < L < 2.5$ r.l.u. (g), (h) 1D cuts along the K direction at different E and \mathbf{Q} across \mathbf{Q}_{IC} . Their corresponding integration ranges are marked by dashed rectangles of the same color in (e). Backgrounds fitted by linear functions are subtracted in the 1D cuts, and the curves are artificially separated along the y axis for clarity. By fitting the peaks with Gaussian functions, we obtain $K = 0.57 \pm 0.01$ and 1.56 ± 0.01 r.l.u.

Figure 2(e) shows the energy dependence of excitations along the $[0, K, 0]$ direction, which reveals two dispersionless excitations at $\mathbf{Q}_{\text{IC}} = (0, K + 0.57, 0)$ with $K = 0, 1$ and a dispersive excitation stemming from the $(0, 2, 0)$ nuclear Bragg peak. The dispersionless excitations at incommensurate wave vectors \mathbf{Q}_{IC} starting from $E = 0.2$ meV must be spin fluctuations since low-energy acoustic phonons must be dispersive and originate from nuclear Bragg peak positions. To test if the dispersive excitation from $(0, 2, 0)$ is indeed an acoustic phonon mode, we plot in Fig. 2(f) the 2D image of excitations along the $[0, K, 2]$ direction. While the \mathbf{Q}_{IC} excitations are no longer present, one can see a similar dispersive mode stemming from the nuclear Bragg peak

$(0, 2, 2)$. By comparing the scattering intensity of these modes with nuclear structure factors, which is proportional to the scattering intensity of acoustic phonon modes [49], we conclude that the dispersive mode is the longitudinal acoustic phonon mode with a sound velocity of ~ 1000 m/s comparable to the sound velocity of UTe measured by Brillouin light scattering [50]. Figures 2(g) and 2(h) show constant-energy cuts along the $[0, K, 0]$ direction at different energies marked in Fig. 2(e). At all energies probed, we see dispersionless incommensurate spin excitations centered around $\mathbf{Q}_{\text{IC}} = (0, K + 0.57 \pm 0.02, 0)$, where $K = 0, 1$, with the dynamic spin correlation length of ~ 12 Å. This is close to the commensurate AF wave vector of $(0, 0.5, 0)$, thus indicating that spin fluctuations in UTe₂ are predominantly AF in nature.

To see how incommensurate spin fluctuations around \mathbf{Q}_{IC} change across T_c and determine if there are strong FM spin fluctuations, we carried out energy scans at wave vectors \mathbf{Q}_1 – \mathbf{Q}_6 as marked in Fig. 2(a) at temperatures $T = 0.3, 2$, and 12 K. Figures 3(a) and 3(b) summarize the key results at the incommensurate wave vectors $\mathbf{Q}_1 = (0, 0.57, 0)$ and $\mathbf{Q}_2 = (0, 1.57, 0)$, respectively. To accurately determine the nuclear incoherent scattering backgrounds from the UTe₂ sample and the Cu sample holder, we chose $\mathbf{Q}_3 = (0, 1.1, 2)$ [Fig. 3(c)] and $\mathbf{Q}_4 = (0, 2, 1)$ [Fig. 3(d)], since these positions are near the incommensurate and FM positions, respectively, but are sufficiently away from the nuclear Bragg peak positions. For possible FM spin fluctuations, we consider nuclear Bragg peak positions $\mathbf{Q}_5 = (0, 1, 1)$ [Fig. 3(e)] and $\mathbf{Q}_6 = (0, 2, 0)$ [Fig. 3(f)].

Figures 3(c) and 3(d) show the nuclear incoherent scattering background at \mathbf{Q}_3 and \mathbf{Q}_4 , respectively. As expected, the scattering is weakly wave vector and temperature dependent between 0.3 and 12 K. The green dashed lines in Figs. 3(a) and 3(b) are measured incoherent background scattering. The incommensurate spin fluctuations are clearly above the background scattering and follow the Bose population factor on warming from 0.3 to 12 K. Figures 3(g) and 3(h) show the temperature dependence of the imaginary part of the dynamic susceptibility $\chi''(E)$ at \mathbf{Q}_1 and \mathbf{Q}_2 , obtained by subtracting the incoherent scattering backgrounds and correcting for the Bose population factor [6]. $\chi''(E)$ at both incommensurate wave vectors increase with increasing energy, but show no dramatic temperature dependence on warming from 0.3 to 2 K across T_c , and to 12 K. This is reminiscent of the temperature dependent $\chi''(E)$ in Sr₂RuO₄ [22–24], but clearly different from spin-singlet unconventional heavy-fermion superconductors such as CeCoIn₅ [55,56], CeCu₂Si₂ [57], etc., where there is a strong enhancement of $\chi''(E)$, termed neutron spin resonance [51–54], in the pink marked energy region below T_c .

Figures 3(e) and 3(f) summarize our attempt to extract FM spin fluctuations in UTe₂, where the green dashed lines

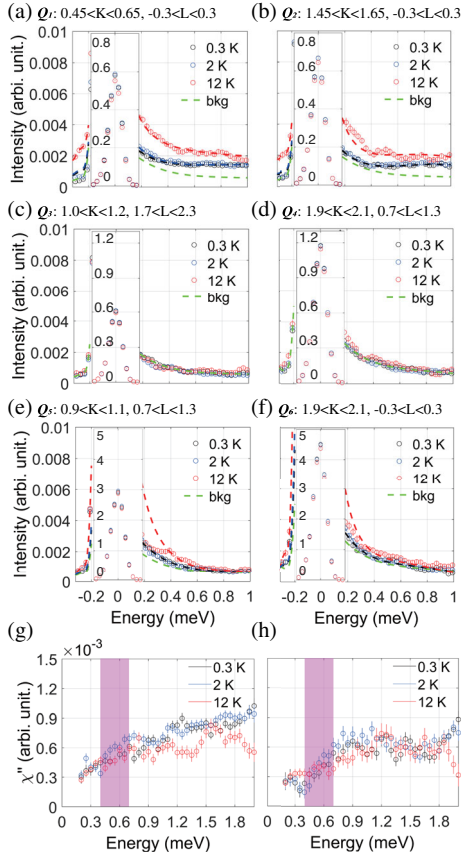


FIG. 3. (a)–(f) Constant- \mathbf{Q} cuts correspond to the \mathbf{Q}_1 – \mathbf{Q}_6 positions marked in Fig. 2(a) at $T = 0.3, 2,$ and 12 K. The insets show the incoherent or Bragg intensity from $E = -0.2$ to 0.2 meV depending on whether a Bragg peak exists at each \mathbf{Q} position. Dashed lines on the neutron energy loss side ($E > 0$ side) are obtained by fitting the $T = 0.3$ K data, which are then scaled up based on the Bose population factor for the 2 and 12 K data. On the neutron energy gain side ($E < 0$), dashed lines are obtained by fitting the 12 K data, which are then scaled down based on the Bose population factor. (g),(h) The $\chi''(E)$ within \mathbf{Q}_1 and \mathbf{Q}_2 , respectively. The pink shadow region highlights the energy range of $3k_B T_c - 5k_B T_c$, where a spin resonance appears below T_c in many spin-singlet unconventional superconductors [51–54].

are incoherent scattering backgrounds measured at \mathbf{Q}_3 and \mathbf{Q}_4 , respectively. Compared with Figs. 3(a) and 3(b) at \mathbf{Q}_{IC} , we see that FM spin fluctuations, if present, are much smaller in magnitude and essentially vanish above ~ 0.7 meV within the errors of our measurements. Although temperature dependence of the scattering suggests the presence of FM spin fluctuations, they do not dominate the spin fluctuation spectra and neutron polarization analysis [25] may be necessary to conclusively identify FM spin fluctuations in UTe_2 .

To understand these results, we have also performed the electronic structure calculations of UTe_2 using the DFT + DMFT method [45–48]. In a heavy-fermion metal such as UTe_2 , there are two potential origins for the wave

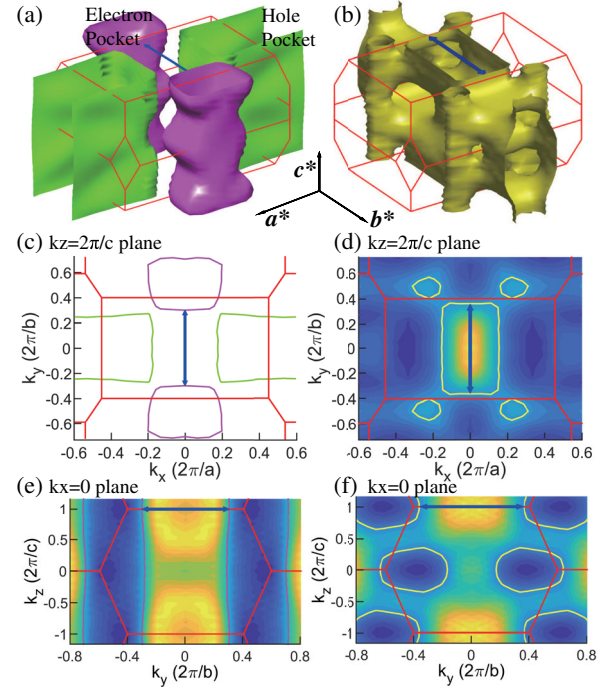


FIG. 4. (a) The 3D Fermi surfaces calculated by using DFT and treating $U - 5f$ electrons as open core states [58]. (b) The 3D Fermi surfaces of $U - 5f$ electrons from DFT + DMFT calculations. Blue arrows on the top edge of the first BZ as well as those in (c)–(f) indicate the spanning wave vector through Fermi surface nesting. (c)–(f) 2D cuts of the band calculation at the $k_z = 2\pi/c$ plane and $k_x = 0$ plane, respectively. In (c)–(f) the BZ is indicated by red lines, and the Fermi level of each band is marked with curves using the same color as used in the 3D plot in (a) and (b).

vector of incommensurate spin fluctuations. One is the RKKY interaction between the $5f$ moments, as appearing in a Kondo lattice model, which is determined by the electronic structure of the spd conduction electrons. For this electronic structure, $U - 5f$ electrons are treated as open core states (similarly via DFT to ThTe_2 [43]), the calculated Fermi surface is shown in Figs. 4(a), 4(c), and 4(e) (see Supplemental Material [49]). Noticeably, the electron momentum transfer across the two purple Fermi pockets is about $0.61b^*$, close to \mathbf{Q}_{IC} observed in the INS experiments. Another potential source for the wave vector of incommensurate spin fluctuations is the Fermi surface nesting of the $U - 5f$ heavy bands, which we have determined using the DFT + DMFT method [49]. The Fermi surface of the heavy bands is shown in Figs. 4(b), 4(d), and 4(f). Specifically, at $k_z = 2\pi/c$, the Fermi surface exhibits a rectangular shape, and the electron momentum transfer across the short edges of the rectangular shape is about $0.72b^*$, which is slightly away from the observed \mathbf{Q}_{IC} . Therefore, the RKKY interaction of the $5f$ moments is likely driving the incommensurate spin fluctuations of UTe_2 , although the nesting of the strongly renormalized f -electron bands at the Fermi energy cannot be ruled out.

Superconductivity in UTe_2 is possibly of odd-parity, chiral p -wave type based on the findings of recent scanning tunneling microscopy measurements [40]. Application of a large hydrostatic pressure on UTe_2 appears to induce an AF quantum critical point [59], indicating the presence of a nearby AF order. Therefore, our observation of incommensurate spin fluctuations close to the AF order wave vector in UTe_2 suggests that the superconductivity here is similar to that of UPt_3 , which also has odd-parity pairing [26–28] and is near a (large-moment) AF ordered phase [60]. The U-based heavy-fermion systems not only have a large spin-orbit coupling (SOC) but also involve Hund’s coupling due to the multiple f orbitals that are involved in the low-energy physics. In the presence of these couplings, a chiral p -wave pairing may develop even though the spin fluctuations are AF due to the large SOC-induced spin space anisotropy [61] or competition between different couplings [62]. These effects are expected to be particularly pronounced in the multiorbital Kondo lattice setting [63,64], as we have evidenced here for UTe_2 . Therefore, our results should stimulate new directions to understand p -wave pairing in the multiorbital Kondo lattice systems [65].

In summary, we have discovered that the dominant spin fluctuations in UTe_2 are incommensurate near AF wave vector and extend to at least 2.6 meV. These results are consistent with DFT + DMFT calculations, indicating that incommensurate spin fluctuations in UTe_2 may arise from the \mathbf{Q} dependence of the RKKY interaction between the $U - 5f$ moments. We expect these incommensurate spin fluctuations to play an important role in the development of the unconventional superconductivity.

The INS work at Rice is supported by the U.S. DOE, BES under Award No. DE-SC0012311 (P. D.). Part of the material characterization efforts at Rice is supported by the Robert A. Welch Foundation Grant No. C-1839 (P. D.). Research at UC San Diego was supported by the U.S. DOE, BES under Award No. DEFG02-04-ER46105 (single crystal growth) and U.S. NSF under Grant No. DMR-1810310 (characterization of physical properties). Work at Los Alamos was carried out under the auspices of the U.S. DOE National Nuclear Security Administration under Award No. 89233218CNA000001 and was supported by the LANL LDRD Program. The theory work at Rice has been supported by the U.S. DOE, BES under Award No. DE-SC0018197 and the Robert A. Welch Foundation Grant No. C-1411. A portion of this research used resources at the Spallation Neutron Source, a DOE Office of Science User Facility operated by ORNL.

*pdai@rice.edu

- [1] J. Bardeen, L. N. Cooper, and J. R. Schrieffer, *Phys. Rev.* **106**, 162 (1957).
 [2] D. J. Scalapino, *Rev. Mod. Phys.* **84**, 1383 (2012).

- [3] P. A. Lee, N. Nagaosa, and X.-G. Wen, *Rev. Mod. Phys.* **78**, 17 (2006).
 [4] Q. Si, R. Yu, and E. Abrahams, *Nat. Rev. Mater.* **1**, 16017 (2016).
 [5] G. R. Stewart, *Adv. Phys.* **66**, 75 (2017).
 [6] P. C. Dai, *Rev. Mod. Phys.* **87**, 855 (2015).
 [7] D. Fay and J. Appel, *Phys. Rev. B* **22**, 3173 (1980).
 [8] A. P. Mackenzie and Y. Maeno, *Rev. Mod. Phys.* **75**, 657 (2003).
 [9] C. Kallin and A. J. Berlinsky, *J. Phys. Condens. Matter* **21**, 164210 (2009).
 [10] D. M. Lee, *Rev. Mod. Phys.* **69**, 645 (1997).
 [11] L. Fu and E. Berg, *Phys. Rev. Lett.* **105**, 097001 (2010).
 [12] M. Sato, *Phys. Rev. B* **81**, 220504(R) (2010).
 [13] X.-L. Qi, T. L. Hughes, and S.-C. Zhang, *Phys. Rev. B* **81**, 134508 (2010).
 [14] M. Sato and Y. Ando, *Rep. Prog. Phys.* **80**, 076501 (2017).
 [15] N. Read and D. Green, *Phys. Rev. B* **61**, 10267 (2000).
 [16] A. Y. Kitaev, *Phys. Usp.* **44**, 131 (2001).
 [17] S. S. Saxena, P. Agarwal, K. Ahilan, F. M. Grosche, R. K. W. Haselwimmer, M. J. Steiner, E. Pugh, I. R. Walker, S. R. Julian, P. Monthoux, G. G. Lonzarich, A. Huxley, I. Sheikin, D. Braithwaite, and J. Flouquet, *Nature (London)* **406**, 587 (2000).
 [18] D. Aoki, A. Huxley, E. Ressouche, D. Braithwaite, J. Flouquet, J.-P. Brison, E. Lhotel, and C. Paulsen, *Nature (London)* **413**, 613 (2001).
 [19] N. T. Huy, A. Gasparini, D. E. de Nijs, Y. Huang, J. C. P. Klaasse, T. Gortenmulder, A. de Visser, A. Hamann, T. Görlach, and H. v. Löhneysen, *Phys. Rev. Lett.* **99**, 067006 (2007).
 [20] A. D. Huxley, S. Raymond, and E. Ressouche, *Phys. Rev. Lett.* **91**, 207201 (2003).
 [21] C. Stock, D. A. Sokolov, P. Bourges, P. H. Tobash, K. Gofryk, F. Ronning, E. D. Bauer, K. C. Rule, and A. D. Huxley, *Phys. Rev. Lett.* **107**, 187202 (2011).
 [22] Y. Sidis, M. Braden, P. Bourges, B. Hennion, S. NishiZaki, Y. Maeno, and Y. Mori, *Phys. Rev. Lett.* **83**, 3320 (1999).
 [23] S. Kunkemöller, P. Steffens, P. Link, Y. Sidis, Z. Q. Mao, Y. Maeno, and M. Braden, *Phys. Rev. Lett.* **118**, 147002 (2017).
 [24] K. Iida, M. Kofu, K. Suzuki, N. Murai, S. Ohira-Kawamura, R. Kajimoto, Y. Inamura, M. Ishikado, S. Hasegawa, T. Masuda, Y. Yoshida, K. Kakurai, K. Machida, and S. Lee, *J. Phys. Soc. Jpn.* **89**, 053702 (2020).
 [25] P. Steffens, Y. Sidis, J. Kulda, Z. Q. Mao, Y. Maeno, I. I. Mazin, and M. Braden, *Phys. Rev. Lett.* **122**, 047004 (2019).
 [26] R. Joynt and L. Taillefer, *Rev. Mod. Phys.* **74**, 235 (2002).
 [27] E. R. Schemm, W. J. Gannon, C. M. Wishne, W. P. Halperin, and A. Kapitulnik, *Science* **345**, 190 (2014).
 [28] K. E. Avers, W. J. Gannon, S. J. Kuhn, W. P. Halperin, J. A. Sauls, L. DeBeer-Schmitt, C. D. Dewhurst, J. Gavilano, G. Nagy, U. Gasser, and M. R. Eskildsen, *Nat. Phys.* **16**, 531 (2020).
 [29] G. Aeppli, E. Bucher, C. Broholm, J. K. Kjems, J. Baumann, and J. Hufnagl, *Phys. Rev. Lett.* **60**, 615 (1988).

- [30] G. Aeppli, D. Bishop, C. Broholm, E. Bucher, K. Siemensmeyer, M. Steiner, and N. Stüsser, *Phys. Rev. Lett.* **63**, 676 (1989).
- [31] S. Ran, C. Eckberg, Q.-P. Ding, Y. Furukawa, T. Metz, S. R. Saha, I.-L. Liu, M. Zic, H. Kim, J. Paglione, and N. P. Butch, *Science* **365**, 684 (2019).
- [32] D. Aoki, A. Nakamura, F. Honda, D. X. Li, Y. Homma, Y. Shimizu, Y. J. Sato, G. Knebel, J.-P. Brison, A. Pourret, D. Braithwaite, G. Lapertot, Q. Niu, M. Vališka, H. Harima, and J. Flouquet, *J. Phys. Soc. Jpn.* **88**, 043702 (2019).
- [33] S. Ran, I.-L. Liu, Y. Suk Eo, D. J. Campbell, P. M. Neves, W. T. Fuhrman, S. R. Saha, C. Eckberg, H. Kim, D. Graf, F. Balakirev, J. Singleton, J. Paglione, and N. P. Butch, *Nat. Phys.* **15**, 1250 (2019).
- [34] S. Imajo, Y. Kohama, A. Miyake, C. Dong, M. Tokunaga, J. Flouquet, K. Kindo, and D. Aoki, *J. Phys. Soc. Jpn.* **88**, 083705 (2019).
- [35] S. Ikeda, H. Sakai, D. Aoki, Y. Homma, E. Yamamoto, A. Nakamura, Y. Shiokawa, Y. Haga, and Y. Onuki, *J. Phys. Soc. Jpn.* **75**, 116 (2006).
- [36] S. Sundar, S. Gheidi, K. Akintola, A. M. Cote, S. R. Dunsiger, S. Ran, N. P. Butch, S. R. Saha, J. Paglione, and J. E. Sonier, *Phys. Rev. B* **100**, 140502(R) (2019).
- [37] N. Tateiwa, T. C. Kobayashi, K. Hanazono, K. Amaya, Y. Haga, R. Settai, and Y. Onuki, *J. Phys. Condens. Matter* **13**, L17 (2001).
- [38] E. D. Bauer, R. P. Dickey, V. S. Zapf, and M. B. Maple, *J. Phys. Condens. Matter* **13**, L759 (2001).
- [39] Y. Tokunaga, H. Sakai, S. Kambe, T. Hattori, N. Higa, G. Nakamine, S. Kitagawa, K. Ishida, A. Nakamura, Y. Shimizu, Y. Homma, D. X. Li, F. Honda, and D. Aoki, *J. Phys. Soc. Jpn.* **88**, 073701 (2019).
- [40] L. Jiao, S. Howard, S. Ran, Z. Wang, J. Olivares Rodriguez, M. Sigrist, Z. Wang, N. P. Butch, and V. Madhavan, *Nature (London)* **579**, 523 (2020).
- [41] I. M. Hayes, D. S. Wei, T. Metz, J. Zhang, Y. Suk Eo, S. Ran, S. R. Saha, J. Collini, N. P. Butch, D. F. Agterberg, A. Kapitulnik, and J. Paglione, [arXiv:2002.02539](https://arxiv.org/abs/2002.02539).
- [42] Y. Xu, Y. Sheng, and Y.-F. Yang, *Phys. Rev. Lett.* **123**, 217002 (2019).
- [43] L. Miao, S. Liu, Y. Xu, E. C. Kotta, C.-J. Kang, S. Ran, J. Paglione, G. Kotliar, N. P. Butch, J. D. Denlinger, and L. A. Wray, *Phys. Rev. Lett.* **124**, 076401 (2020).
- [44] J. P. Perdew, K. Burke, and M. Ernzerhof, *Phys. Rev. Lett.* **77**, 3865 (1996).
- [45] A. Georges, G. Kotliar, W. Krauth, and M. J. Rozenberg, *Rev. Mod. Phys.* **68**, 13 (1996).
- [46] G. Kotliar, S. Y. Savrasov, K. Haule, V. S. Oudovenko, O. Parcollet, and C. A. Marianetti, *Rev. Mod. Phys.* **78**, 865 (2006).
- [47] K. Haule, C.-H. Yee, and K. Kim, *Phys. Rev. B* **81**, 195107 (2010).
- [48] R. M. Tutchtton, W.-t. Chiu, R. C. Albers, G. Kotliar, and J.-X. Zhu, *Phys. Rev. B* **101**, 245156 (2020).
- [49] See Supplemental Material at <http://link.aps.org/supplemental/10.1103/PhysRevLett.125.237003> for additional data and analysis.
- [50] M. Mendik and P. Wachter, *Physica (Amsterdam)* **190B**, 72 (1993).
- [51] M. Eschrig, *Adv. Phys.* **55**, 47 (2006).
- [52] S. D. Wilson, P. Dai, S. Li, S. Chi, H. J. Kang, and J. W. Lynn, *Nature (London)* **442**, 59 (2006).
- [53] G. Yu, Y. Li, E. M. Motoyama, and M. Greven, *Nat. Phys.* **5**, 873 (2009).
- [54] D. S. Inosov, J. T. Park, A. Charnukha, Y. Li, A. V. Boris, B. Keimer, and V. Hinkov, *Phys. Rev. B* **83**, 214520 (2011).
- [55] C. Stock, C. Broholm, J. Hudis, H. J. Kang, and C. Petrovic, *Phys. Rev. Lett.* **100**, 087001 (2008).
- [56] Y. Song, W. Wang, J. S. Van Dyke, N. Pouse, S. Ran, D. Yazici, A. Schneidewind, P. Čermák, Y. Qiu, M. B. Maple, D. K. Morr, and P. Dai, *Commun. Phys.* **3**, 98 (2020).
- [57] O. Stockert, J. Arndt, E. Faulhaber, C. Geibel, H. S. Jeevan, S. Kirchner, M. Loewenhaupt, K. Schmalzl, W. Schmidt, Q. Si, and F. Steglich, *Nat. Phys.* **7**, 119 (2011).
- [58] P. Blaha, K. Schwarz, G. K. H. Madsen, D. Kvasnicka, J. Luitz, R. Laskowski, F. Tran, and L. Marks, in *An Augmented Plane Wave + Local Orbitals Program for Calculating Crystal Properties*, edited by K. Schwarz (Technische Universität at Wien, Austria, 2001).
- [59] S. M. Thomas, F. B. Santos, M. H. Christensen, T. Asaba, F. Ronning, J. D. Thompson, E. D. Bauer, R. M. Fernandes, G. Fabbris, and P. F. S. Rosa, *Sci. Adv.* **6**, eabc8709 (2020).
- [60] A. de Visser, M. J. Graf, P. Estrela, A. Amato, C. Baines, D. Andreica, F. N. Gygax, and A. Schenck, *Phys. Rev. Lett.* **85**, 3005 (2000).
- [61] T. Kuwabara and M. Ogata, *Phys. Rev. Lett.* **85**, 4586 (2000).
- [62] Z. Y. Meng, Y. B. Kim, and H.-Y. Kee, *Phys. Rev. Lett.* **113**, 177003 (2014).
- [63] Q. Y. Chen, X. B. Luo, D. H. Xie, M. L. Li, X. Y. Ji, R. Zhou, Y. B. Huang, W. Zhang, W. Feng, Y. Zhang, L. Huang, Q. Q. Hao, Q. Liu, X. G. Zhu, Y. Liu, P. Zhang, X. C. Lai, Q. Si, and S. Y. Tan, *Phys. Rev. Lett.* **123**, 106402 (2019).
- [64] I. Giannakis, J. Leshen, M. Kawai, S. Ran, C.-J. Kang, S. R. Saha, Y. Zhao, Z. Xu, J. W. Lynn, L. Miao, L. Andrew Wray, G. Kotliar, N. P. Butch, and P. Aynajian, *Sci. Adv.* **5**, eaaw9061 (2019).
- [65] R. Yu, H. Hu, E. M. Nica, J.-X. Zhu, and Q. Si, [arXiv:2007.00181](https://arxiv.org/abs/2007.00181).